Direct Method for Optimization of a Centrifugal Compressor Vaneless Diffuser

Yu-Tai Lee
Naval Surface Warfare Center,
Carderock Division,
West Bethesda, MD 20817

Lin Luo
The Pennsylvania State University,
University Park, PA 16801

Thomas W. Bein
Naval Surface Warfare Center,
Annapolis Detachment,
Annapolis, MD 21402

A Direct Method for Optimization (DMO) is developed for investigating pressure rise and energy loss in a vaneless diffuser of a generic compressor used in shipboard air-conditioning systems. The scheme uses Reynolds-Averaged Navier–Stokes (RANS) results and evaluates gradients of a predetermined objective function. The current Direct Method for Optimization differs from the popular Inverse Design Method in the process of obtaining final configurations and in the final configurations obtained. The Direct Method for Optimization achieves a final shape from maximizing/minimizing a nonlinear function, i.e., the objective function. Both gradient and nongradient Direct Methods for Optimization are compared with respect to accuracy and efficiency. The coupled DMO/RANS optimization code is benchmarked using a plane turbulent diffuser also investigated by Zhang et al. using an adjoint method. The benchmark indicates that if a global optimum exists, the result should be independent of the methodologies or design parameters used. The DMO/RANS method is applied to redesign a three-dimensional centrifugal vaneless diffuser used in a modern generic compressor. The objective function is a composite function of the diffuser's pressure rise and total energy loss. The new optimum diffuser has a minimum width at a location far beyond the conventional diffuser pinch point. The new diffuser also provides an efficient section for pressure recovery, which takes place after the minimum width location. Test data for the new diffuser validate the current approach at the design condition. Furthermore, improved performance is also recorded experimentally at off-design conditions for the optimized diffuser.
[DOI: 10.1115/1.308571]

Introduction

Diffusers, functioning as pressure-recovery devices, are absolutely essential for good turbomachinery performance. Diffuser performance is governed by geometric and aerodynamic parameters.

Diffusers are categorized as channel, conical, and annular types [1]. The annular diffuser with radial inflow and radial outflow is also known as a vaneless diffuser. Vaneless diffusers are employed for centrifugal compressors and pumps as exemplified in Fig. 1 for an air-conditioning compressor. Although the compressor in Fig. 1 was designed using a state-of-the-art turbomachinery design tool, it still shows a large discrepancy between the predicted compressor efficiency and the measured efficiency. Further research [2] indicates that the faulty prediction occurs at the compressor's diffuser and volute. Improved computational techniques were therefore developed [3] to investigate the flow features within these components. In order to refine each component's performance further in an efficient manner, development of an optimization method is desirable.

The mathematical requirement of an optimization scheme is to maximize (or minimize) an objective (or an output) function, which represents the parameter of interest from a mathematical model of the problem. As we know, in order to determine the minimum value of a function, multidimensional mapping of the function is impractical. Thus, an optimization procedure is required that is considerably more efficient than multidimensional mapping.

Many attempts and successes exist in the literature on the topics of optimization using computational-fluid-dynamic (CFD) methods. Among these efforts, the adjoint method and the gradient-based method are the most popular approaches. The adjoint method is represented by Baysal and Eleshaky [4] and Reuther and Jameson [5] for wing shapes, and by Cabuk and Modi [6] and Zhang et al. [7] for plane diffusers. The gradient-based method is represented by Panting [8] for aeroengine optimization, Mrsa [9] for nozzle design, and Koller et al. [10] for compressor blade shaping. The adjoint method requires derivation of the adjoint equations for each new problem. Extension of the adjoint method

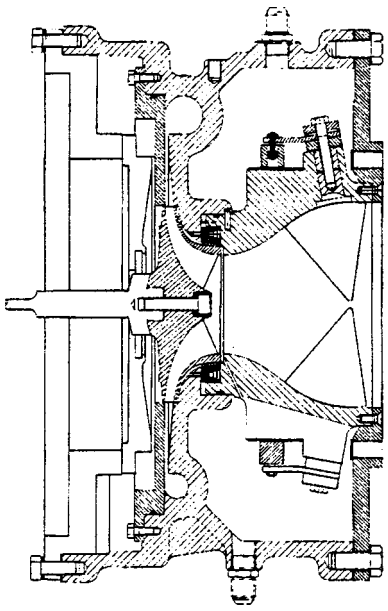

Fig. 1 Generic air-conditioning compressor

Contributed by the International Gas Turbine Institute and presented at the 45th International Gas Turbine and Aeroengine Congress and Exhibition, Munich, Germany, May 8–11, 2000. Manuscript received by the International Gas Turbine Institute February 2000. Paper No. 2000-GT-453. Review Chair: D. Ballal.

from laminar to turbulent flow is not a trivial task, and the adjoint equations for more sophisticated turbulence models can be quite challenging. Furthermore, the objective function for an adjoint method may lack uniqueness [7], which affects the final optimum solution.

In this paper we present a more heuristic approach and apply it to a general diffuser optimization. The method developed is called the Direct Method for Optimization (DMO) and is a gradient-based approach. The DMO is coupled with a CFD method and a regridding approach to iteratively march to the optimized shape.

Direct Method for Optimization

The mathematical representation of an optimization problem can be formulated as follows. Given a predetermined input vector $\vec{x}$ and an objective function (or a parameter of interest) $f(\vec{x})$ for the problem, the DMO is to find an optimal value $\vec{x}^*$ such that $f(\vec{x}^*) \leqslant f(\vec{x})$, provided the constraint $\vec{x}_{\min} \leqslant \vec{x} \leqslant \vec{x}_{\max}$.

For the stated problem, a local minimum can be found through a gradient vector,

$$g_i = \frac{\partial f(\vec{x})}{\partial x_i} \tag{1}$$

where $\vec{x}=(x_i)$ and $\vec{g}=(g_i)$, $i=1,\ldots,n$ and n is the dimension of the problem. The general objective function $f(\vec{x})$ can be approximated as a multidimensional quadratic function,

$$f(\vec{x}) \approx \frac{1}{2}\vec{x}\cdot[A]\cdot\vec{x} - \vec{b}\cdot\vec{x} + c \tag{2}$$

where $[A]$ is the second partial derivative (or the Hessian) matrix of f. In order to convert the multidimensional function to a one-dimensional problem and use a line-minimization scheme, an optimal direction must be determined. This direction has been proven [11] to be one of a conjugate pair, called a conjugate set, which are the bases for selecting the marching direction in the direction set method [11]. For functions that are not exactly quadratic forms, as shown in Eq. (2), repeated use of the mutually conjugate line-minimization directions will, in due course, converge quadratically to the desired minimum.

Furthermore, if the direction of the line-minimization is constructed to be conjugate to the direction used in the previous iteration or to all directions traversed in all previous iterations, the conjugate gradient algorithm is obtained. In this paper, the Polak–Ribiere conjugate gradient scheme [12] is adapted. If $\vec{u}$ is such a conjugate direction, the Polak–Ribiere scheme is given as

$$\begin{aligned} \vec{u}_1 &= -\vec{g}(\vec{x}_1) \\ \vec{u}_{k+1} &= -\vec{g}(\vec{x}_{k+1}) - \gamma_{k+1}\vec{g}(\vec{x}_k) \\ \gamma_{k+1} &= \frac{\vec{g}(\vec{x}_{k+1})\cdot\{\vec{g}(\vec{x}_{k+1}) - \vec{g}(\vec{x}_k)\}}{\vec{g}(\vec{x}_k)\cdot\vec{g}(\vec{x}_k)} \end{aligned} \tag{3}$$

where the subscript represents the iteration number.

DMO on Vaneless Diffuser

Using the aforementioned Polak–Ribiere conjugate gradient scheme (Eq. (3)), the geometric and flow constraints of the vaneless diffuser of the given compressor are depicted in Fig. 2. The inlet condition is fixed by a constant mass flow rate and a constant inflow angle. The shape of the diffuser shroud is represented by a cubic spline. The number of design stations, which correspond to the dimension n of the current optimization problem, is flexible. In this paper, we use 3 and 6 points to demonstrate the robustness of the methodology. Figure 2 shows the six-point design stations. Segment S0 of the shroud curve in Fig. 2 is fixed as an inlet-shape constraint. All the other shroud locations, including the one at the diffuser exit, are to be optimized.

For the current diffuser problem, the objective function f is defined as

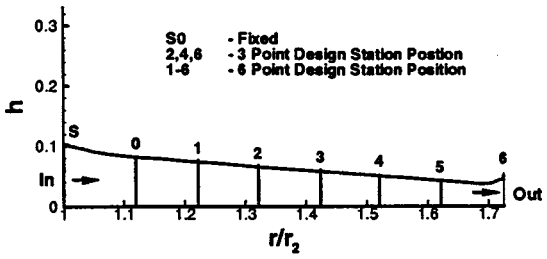

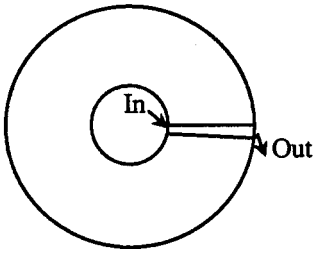

Fig. 2 Schematics of the vaneless diffuser geometry

$$f(\vec{h}) = \beta\omega - \alpha C_p$$

$$\omega = \frac{p_{t3} - p_{t2}}{1/2\rho_2 U_2^2}; \quad C_p = \frac{p_{s3} - p_{s2}}{1/2\rho_2 U_2^2} \tag{4}$$

where $\vec{h}=(h_i)$, $i=1,\ldots,n$ represents the diffuser width vector at the design stations and is normalized by the impeller radius, ω is the total pressure loss coefficient, C_p is the static pressure rise coefficient, p_{s2} and p_{s3} are the inlet and outlet mass-averaged static pressures, p_{t2} and p_{t3} are the mass-averaged inlet and outlet total pressures, α and β are weighting coefficients, and ρ_2 and U_2 are inlet density and velocity. Equation (4) indicates that the objective function f is a composite function of the diffuser static pressure rise and the total pressure loss and is weighted by the coefficients α and β. All the parameters studied are nonlinear functions of $\vec{h}$. The static and total pressure distributions are obtained by solving the RANS equations.

The complete optimization procedure is described as follows:

1 Problem definition: including input vector $\vec{h}$, constraints, and objective function $f(\vec{h})$;

2 Initialization of optimization calculation: including normalization of $\vec{h}$ and variable limitation;

3 Flow prediction: including solving the RANS equations with an initial grid and calculating relevant $f(\vec{h})$;

4 Preparation of optimization calculation: including evaluation of gradient vector $\vec{g}$ and determination of mutually conjugate directions;

5 Optimization calculation: including bracketing the minimum, conducting the line minimization and optimization iteration;

6 Convergence check: checking the convergence of the design variables. If the design requirements are met, the process is complete. Otherwise, the calculation continues to the next step.

7 CFD regridding: including defining the new boundary surfaces and their smoothing, and interior grid movement. Return to step (3) for another gradient iteration.

The gradient vector $g(\vec{h})$ is obtained by

$$g(h_i) = \frac{f(h_i + \Delta h_i) - f(h_i)}{\Delta h_i}, \quad (i=1,\ldots,n) \tag{5}$$

Evaluating these gradients takes enormous computational effort. Thus, in this paper, two other nonlinear non-gradient-based optimization schemes are also examined for the present vaneless diffuser case. These are the downhill simplex method [13] and the Powell method [14]. Although there is no requirement to evaluate the gradient of the objective function f for these latter schemes, the total number of iteration cycles needed to obtain a minimum may be large. If, however, the function f does not lead to quadratic convergence, these nongradient, more heuristic schemes become more competitive in terms of computational effort and accuracy. A numerical illustration of the aforementioned procedure is given in the appendix for a two-dimensional plane diffuser optimization discussed in the Prediction Results section.

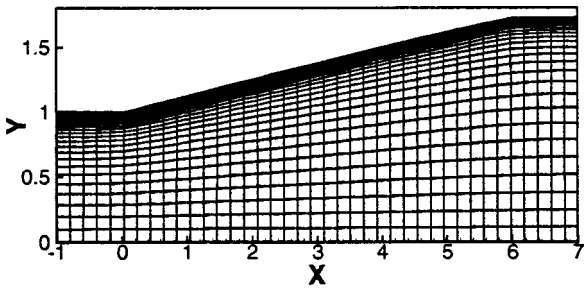

Fig. 3 Typical computational grid for turbulent plane diffuser

RANS Solution Method

Computational Scheme. The governing equations, including the continuity, momentum, and energy equations, for compressible flow are solved with a two-equation $k-\varepsilon$ turbulence model for the diffuser flow. The governing equations in curvilinear coordinates are written as:

$$\frac{1}{J}\frac{\partial}{\partial t}(\rho q)=\frac{\partial}{\partial \xi_i}\left(-\rho U_i q+\mu_{\text{eff}} G_{ij}\frac{\partial q}{\partial \xi_i}\right)+S_q \tag{6}$$

where $q=[1,u_x,u_y,u_z,h,k,\varepsilon]$ and ρ,J,U_i,G_{ij} represent fluid density, the Jacobian of the coordinate transformation, transformed velocities, and diffusion metrics, respectively. The effective viscosity μ_{eff} represents a sum of the laminar viscosity μ and the turbulent eddy viscosity μ_t, re-scaled by a turbulence Prandtl number or Schmidt number. The turbulent eddy viscosity $\mu_t=\rho C_\mu k^2/\varepsilon$ and $C_\mu=0.09$.

Finite-difference approximations are used to discretize the transport equations on nonstaggered grid systems. An upwind scheme is used to model the convective terms and a central differencing formula is used for the viscous and source terms of Eq. (6). For turbulence quantities, the convection process is modeled by an upwind scheme. A pressure-based predictor/corrector solution procedure [15] is employed to achieve velocity-pressure coupling. The discretized systems are solved by an implicit Euler time-marching scheme. The numerical solutions are considered converged when the residuals of each discretized equation have dropped by five orders of magnitude from their initial values. The computational technique and results for a centrifugal compressor's vaneless diffuser and volute have been demonstrated in Lee and Bein [3]. In order to minimize the RANS computational effort for the present vaneless diffuser optimization, axisymmetric calculations are performed with a prescribed inflow angle, total pressure, total temperature, and a diffuser exit pressure. The diffuser exit pressure prescribed at the exit mid-width is obtained through iteration until the design mass flow rate is maintained.

Grid Movement. Regridding en route to the optimized shape is completed using an algebraic grid movement strategy. After a new shroud shape is generated by the DMO, the points on the shroud boundary are moved to the new shape, and interior grid points are moved proportionally based on the original grid distribution. Grid smoothing is employed to compensate for large boundary movement and inadvertent grid-line crossing.

Prediction Results From Optimization Calculations

Plane Diffusers in Turbulent Flow. Cabuk and Modi [6] and Zhang et al. [7] have studied plane diffuser optimization for laminar and turbulent flows using the adjoint method. They use an objective function of the flow-weighted static-pressure rise between the diffuser inlet and outlet. For the turbulent plane diffuser, Zhang studied a geometry with a ratio of diffuser length to inlet width equal to 6. As Fig. 3 shows, a head-pipe and a tail-pipe with lengths equal to the inlet width were added to the entrance and exit. The grid shown in Fig. 3, with dimensions of 40×30, was used for the incompressible turbulent-flow computations in this paper and is comparable to the grid used by Zhang. The Reynolds number is 10,000 based on the mean inlet velocity and inlet width. The inflow is assumed to have a fully developed power-law velocity distribution. The initial diffuser shape, a constant width channel, differs from that used by Zhang, a cosine type with an amplitude of 0.33. In order to compare the current approach to Zhang's, α is set to unity and β to zero in Eq. (4). Zhang shows results based on two different design functions in his adjoint representation of the objective function: a product form,

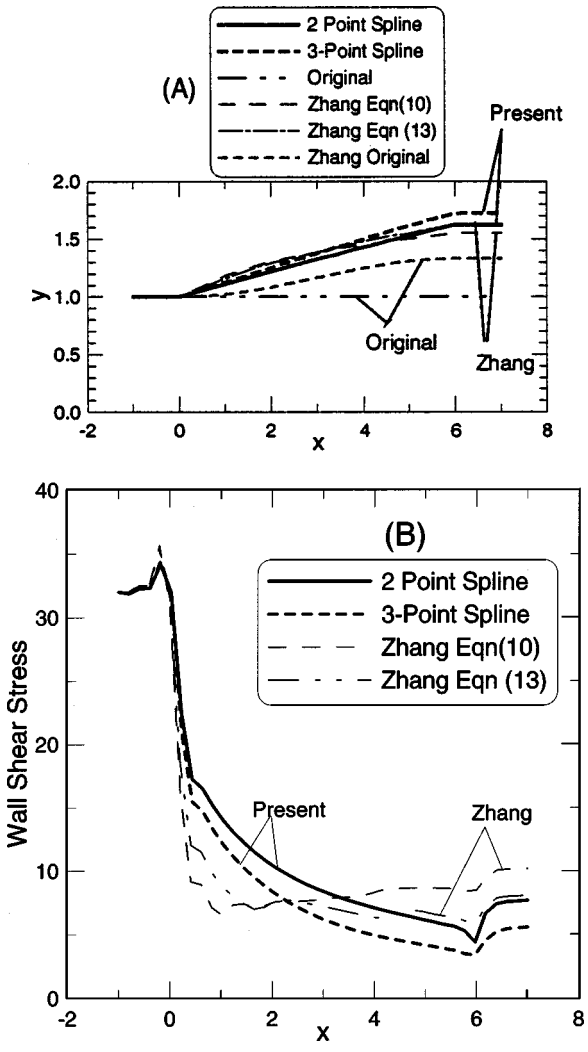

Fig. 4 Optimization of plane diffuser and comparison with [7]: (*A*) diffuser shapes; (*B*) wall shear stress

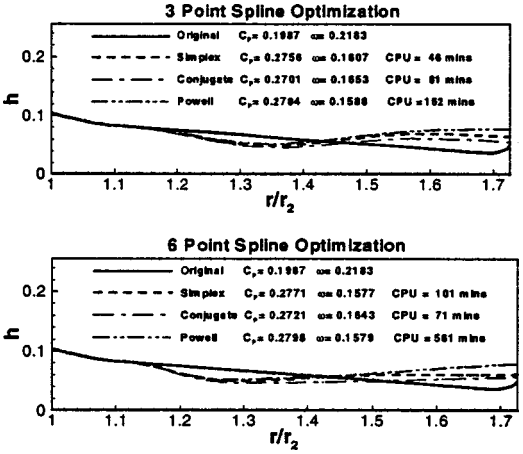

Fig. 5 Optimization of vaneless diffuser: (*A*) three-point spline; (*B*) six-point spline (C_p=static pressure rise, ω=total pressure loss)

and a shear ratio form (identified as Eq. (10) and Eq. (13), respectively, in his paper). The choice of the different design functions is due to the nonuniqueness of the problem.

Prediction results based on the present DMO/RANS calculation are shown in Fig. 4 and compared to Zhang's results. A two-point spline calculation and a three-point spline calculation were used with the current approach. The design locations are at $x=3$ and 6 for the two-point spline and at $x=2$, 4, and 6 for the three-point spline. The final diffuser curves are plotted in Fig. 4(*a*) and the wall shear distributions are depicted in Fig. 4(*b*). The variation of the objective function between successive iterations is monitored and compared to a prescribed tolerance. For the plane diffuser, the tolerance is set to 10^{-5}. The complete optimization calculation for the two-point spline takes 110 iterations and 5 gradient cycles. Although the two-point spline agrees better with Zhang's shear form result, the three-point spline produces a slightly larger exit area, higher pressure recovery and lower wall shear. The abrupt drop in shear stress at the end of the inlet head-pipe, which exists in all the solutions, is associated with a discontinuity in wall slope and a divergence of the wall shape at that location. Limited by the solution accuracy of each optimization approach and their constraints, the present comparison indicates that different methods or different design parameters lead to similar final global optimum shapes, as they should if indeed a unique optimum exists.

Vaneless Diffuser of the Generic Compressor. The vaneless diffuser of the generic compressor, as shown in Figs. 1 and 2, starts at the impeller exit radius of $r_2=12.24$ cm (4.82 in). The diffuser inlet velocity is 128 m/s (420 ft/s) and the mass flow at the design condition is 4 kg/s (8.8 lbm/s). The diffuser inflow Mach number is 1.05 and the flow angle is estimated to be 79.5 deg from radial. The Reynolds number based on r_2 and the diffuser inlet velocity is 3.1×10^7. The diffuser has a length of $r_3/r_2=1.725$ and an inlet width of $h_2=0.104$. The original diffuser has a flat hub (front plate) and a curved shroud (back plate). The current optimization design is performed at the design condition with the following geometrical constraints: The diffuser length and the inlet width are kept constant; and the initial section of the shroud curve, i.e., the segment S0 in Fig. 2, is fixed. Station 0 is close to the conventional pinch location. In order to minimize the modification of the compressor front plate where the transmission and the motor are located, the diffuser hub surface is maintained as a fixed flat surface.

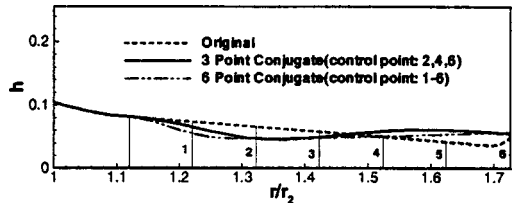

Fig. 6 Comparison of three-point and six-point spline shapes

The optimization results for the vaneless diffuser are shown in Figs. 5–11. Figure 5 compares the original and final shroud curves obtained from the conjugate gradient method and the nongradient downhill simplex and Powell methods with both weighting functions α and β equal to unity. Both the three-point spline and six-point spline are used to study the impact of the number of design dimensions. The curve obtained from the three-point conjugate method is plotted against that from the six-point conjugate method in Fig. 6. The additional design stations at locations 1, 3, and 5 provide an extra level of control for reaching the final optimum shroud curve. Since the simplex and the Powell methods treat the conditions at the endpoint (i.e., the diffuser exit) somewhat differently than the conjugate gradient method, they produce a larger exit width. Because of the smaller exit width produced by the conjugate gradient method, the compressor test for a new diffuser adopts the resultant curve obtained from the conjugate gradient calculation without changing the volute configuration. The static pressure rise C_p, total pressure loss ω, and total CPU time used (in minutes) for each calculation are also shown in Fig. 5. The variations of the predicted flow parameters for all cases studied here are within 3.5 percent for C_p and 4.7 percent for ω. The computational time indicates that the conjugate gradient method is a more efficient scheme for the six-point optimization.

The weighting coefficients α and β in Eq. (4) are factors for controlling the importance of C_p and ω to the final optimum result. Separate calculations using the conjugate gradient method were carried out by setting (*i*) $\alpha=1$ and $\beta=1$; (*ii*) $\alpha=1$ and $\beta=3$; and (*iii*) $\alpha=3$ and $\beta=1$. The optimum shroud curves from these calculations, shown in Fig. 7, indicate that the equal-weight approach is as good as other weights for C_p and ω. Therefore α and β are chosen to be unity in all other calculations.

Figure 8 shows the grids used for the original and modified

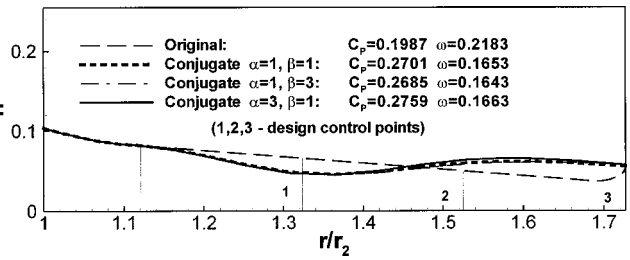

Fig. 7 Impact of the weighting coefficients in Eq. (4)

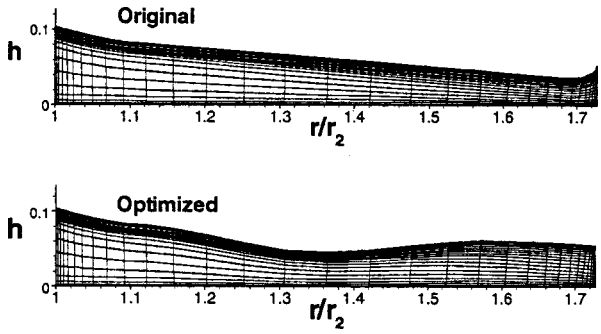

Fig. 8 Computational grids for the original shape and the final shape using conjugate gradient method

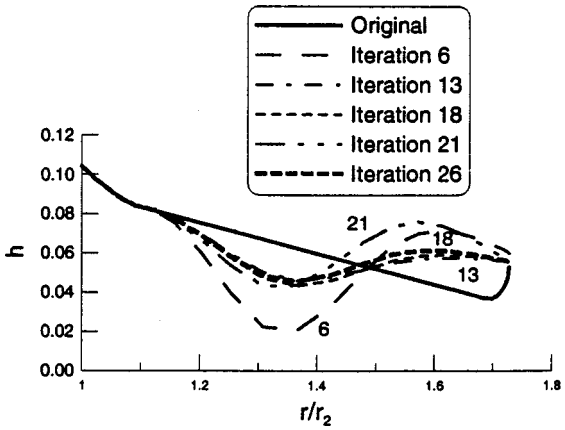

Fig. 9 Selected intermediate shroud shapes through 26 iterations from the original curve

diffusers based on the six-point gradient calculation. The grids have dimensions of $21\times31\times3$ (in the h, r, and θ directions). A clustered grid is used near the shroud surface.

Figure 9 shows variations of the shroud curves at intermediate steps during the conjugate gradient calculation. The complete optimization is completed in 26 iterations and 2 gradient cycles with a tolerance equal to 10^{-3}. Although the plotting scale of the ordinate has been magnified, Fig. 9 shows the robustness of the current scheme, which is capable of correctly steering the prediction after overshooting the final result.

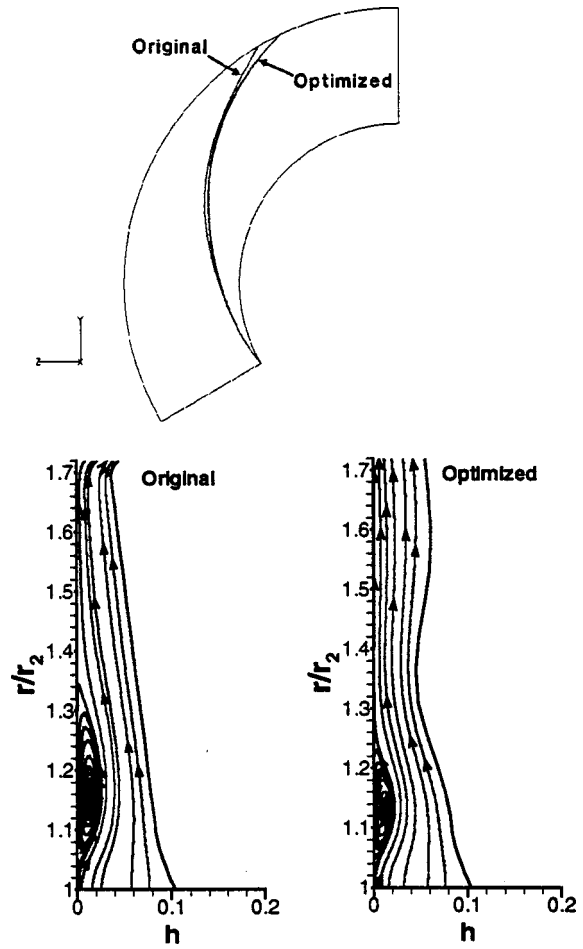

Fig. 10 Predicted flow path: (*A*) on the front plate; (*B*) on a radial section

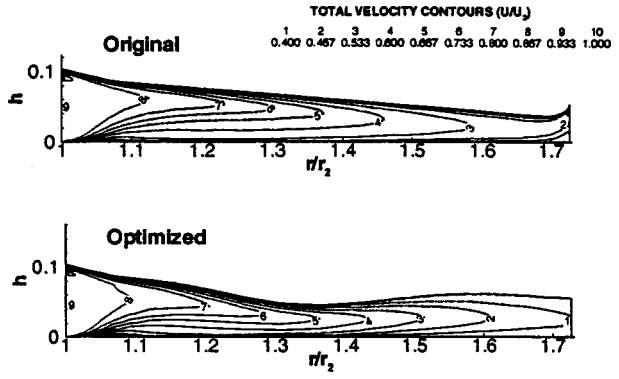

Fig. 11 Predicted total velocity contours

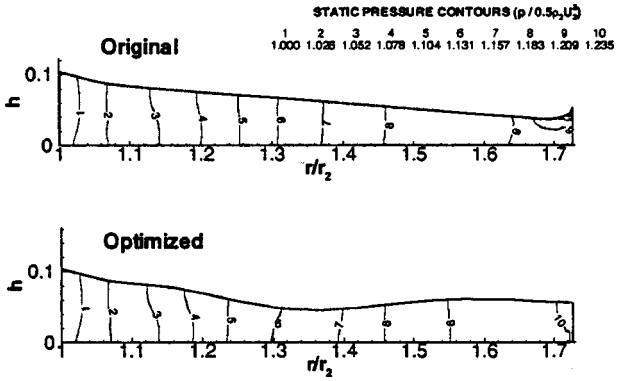

Fig. 12 Predicted static pressure contours

The flow path near the flat hub surface is drawn in Fig. 10(*a*) for the original diffuser and for the modified diffuser from the six-point conjugate gradient calculation. The primary differences in flow angle between the two cases occur near $r/r_2=1.25$ and in the exit area. A view of the flow in a radial section is shown in Fig. 10(*b*). For the original diffuser, the flow separates near the inner radius. Although the flow also separates for the optimized diffuser, the separation region is reduced in size due to the converging shroud curve. The optimization does not completely eliminate the flow separation due to the geometric constraint of the shroud inlet curve, i.e., the section S0 in Fig. 2. A dramatic change in flow angle occurs near the diffuser exit, as shown in Fig. 10(*a*). The optimized shape directs the flow into the volute in a much smoother pattern due to the reduced flow angle.

The velocity and static-pressure distributions along the original and optimized diffusers are shown in Figs. 11 and 12. The convergence of the shroud up to $r/r_2=1.3$ differs from the conventional concept of locating the vaneless diffuser's pinch point within $r/r_2=1.10$ to 1.15. The flow in the optimized diffuser decelerates slower in the radial direction decreasing the effect of the flow separation (Fig. 10(*b*)). The optimized diffuser, however, decelerates the flow faster overall (Fig. 11). This efficient decelerating flow within the diverging shroud (between $r/r_2=1.3$ and 1.7) of the optimized diffuser provides a more efficient mechanism for pressure recovery as shown in the static pressure contours of Fig. 12. The averaged exit Mach number for both diffusers is 0.45.

Experimental Results of the Generic Compressor. Compressor tests were conducted using the original diffuser and the optimum diffuser obtained from the six-point conjugate gradient calculation. The compressor is installed in a shipboard air-

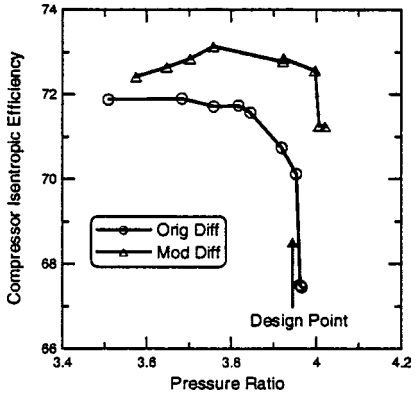

Fig. 13 Measured compressor efficiency for the original and the modified diffusers

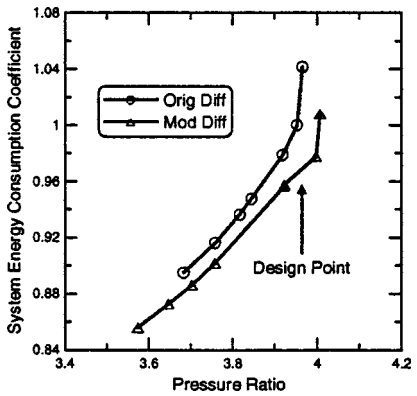

Fig. 14 Measured system energy consumption for the original and the modified diffusers

conditioning system. The compressor performance map was obtained by fixing the impeller speed at 15,160 rpm, the suction conditions and the inlet guide vane positions (fully open), and varying the condensing conditions. Measured data are shown in Figs. 13 and 14 for compressor isentropic efficiency and system energy consumption coefficient versus the ratio of the discharge pressure to the suction pressure. The system energy consumption coefficient is a ratio of the total system energy consumed at various conditions to the consumed energy at the design point for the original diffuser. Due to the current diffuser modification, the compressor efficiency is increased by 2 to 3 percent at the design point and by 1 to 5 percent at off-design conditions. Since the inefficient volute flow remains, the overall compressor efficiency stays relatively low even with the modified diffuser. System energy consumption is reduced by 3 percent at the design point and by 1–7 percent at off-design conditions. These test data support the present optimization results for the vaneless diffuser.

Conclusions

A nonlinear Direct Method for Optimization (DMO) is developed for two-dimensional plane diffusers and three-dimensional vaneless diffusers. The method, coupled with a Reynolds-Averaged Navier–Stokes (RANS) solution method, optimizes a composite objective function of flow parameters which include the diffuser's static-pressure rise and total-pressure loss.

The developed DMO is validated by comparing results to those obtained from an adjoint approach for a plane turbulent diffuser. Limited by the solution accuracy of each optimization approach and their constraints, the comparison between the current solutions and the solutions obtained from the adjoint method indicates that different methods and different design parameters in the objective function lead to similar final optimum shapes.

The current DMO/RANS method is also used to redesign a three-dimensional vaneless diffuser whose original shape was obtained using a state-of-the-art turbomachinery design tool. The final optimum shape from a six-point conjugate gradient calculation shows a converging–diverging shroud. The minimum width occurs at a location far beyond the conventional pinch point. The iteration cycle of the DMO/RANS coupling proceeds along conjugate directions, not only to minimize the objection function, but also to improve the general flow features through a correct selection of the objective function. The theoretically predicted optimum diffuser shape was validated by experiments, both at the design and off-design conditions, to be superior to the original diffuser shape.

Acknowledgments

This work was sponsored by the Shipboard Energy Conservation Program administrated at the Annapolis Laboratory of the Naval Surface Warfare Center. The program manager at the Chief of Naval Operations, Code N420C, is Mr. H. Hodgkins. The program manager at the Carderock Division, Naval Surface Warfare Center is Mr. W. Stoffel. Partial support was provided by the Office of Naval Research (Program Element PE 602121) under the Machinery Systems Task. The program monitor is LCDR F. Novak. The authors are indebted to Messrs. M. Tse, C. Engstrom, and J. M. Loellbach for their help in preparing the final manuscript. Comments from the reviewers and Dr. M. J. Miller are also greatly appreciated.

Nomenclature

$[A]$ = Hessian matrix
$\vec{b}$ = coefficient vector
c, C_μ = constant coefficients
C_p = static pressure rise coefficient
f = objective function
$\vec{g}$ = gradient vector
G_{ij} = diffusion matrix
$\vec{h}$ = diffuser width vector, normalized by r_2
J = Jacobian of coordinate transformation
k = turbulent kinetic energy
n = vector length or dimension
p, p_s = static pressure
p_t = total pressure
q = dependent variable matrix
r = radius
S_q = source term
t = time
$\vec{u}$ = vector representing optimization direction
U_i = velocity components
x, y = coordinates
$\vec{x}, \vec{x}^*$ = input vector and optimum value of $\vec{x}$
α, β, γ = coefficients
ε = turbulence dissipation
λ = line minimization coefficient
$\mu, \mu_t, \mu_{\text{eff}}$ = laminar, turbulent and effective viscosities
θ = tangential
ρ = density and inlet density
ω = total pressure loss coefficient
ξ_i = transformed coordinates

Subscripts

2 = impeller exit
3 = dffuser exit
k = iteration

Appendix

Numerical Illustration of DMO for Plane Diffusers. In order to illustrate the DMO procedure, a numerical example for a complete gradient iteration is depicted as follows for the plane diffuser (shown in Fig. 3). As described in the Prediction Results section for the plane diffusers, Eq. (4) is simplified to $f(\vec{h}) = -C_p$. For the two-point spline calculation shown in Fig. 4, there are two design stations located at $\vec{x}=(3,6)$ and $n=2$. Results from the seven-step optimization procedure (mentioned right before Eq. (5)) after the first gradient cycle are as follows.

1 Initialize input vector or diffuser half width vector $\vec{h}=(1.0,1.0)$. After the first gradient cycle the half width vector is $\vec{h}=(1.0385,1.5895)$ and Fig. 15 shows its spline-fitted shape;

2 Constraint is set to be $0 \leqslant h_i \leqslant 3h_0$, where h_0 is the half width at $x=0$;

3 Flow prediction is performed based on the grid shown in Fig. 15. The predicted $f(\vec{h})=0.1884$;

4 Gradient vector $\vec{g}$ is calculated using Eq. (5) by perturbing the local diffuser half width using $\Delta h=0.1$. Figure 16 shows two perturbed diffuser shapes with their computational grids for evaluations of each component of $\vec{g}$. The predicted gradient vector is $\vec{g}=(0.2229,0.1789)$;

5 Equation (3) calculates the conjugate direction from the predicted $\vec{g}$ of step 4. The line minimization locates $\vec{h}_{k+1}=\vec{h}_k+\lambda_k\vec{u}_k$ for minimum $f(\vec{h}_{k+1})$, where k is an iteration number and λ is a line minimization coefficient [11]. After the first gradient cycle, $\vec{h}_k=(1.0385,1.5895)$, $\vec{u}_k=(0.3601,0.1233)$, $\lambda_k=1.1209$ and $\vec{h}_{k+1}=(1.4421,1.7276)$ and $f(\vec{h}_{k+1})=0.2679$;

6 Check the constraint condition specified in step 2. If the condition is satisfied, continue to next step. Otherwise, reset $f(\vec{h})$ to be a large value and continue to next step;

7 Check the convergence for the CFD solution. If $|(f(\vec{h}_{k+1})-f(\vec{h}_k))/f(\vec{h}_{k+1})| \leqslant \varepsilon$, the calculation is complete. Otherwise, use $\vec{h}_{k+1}$ as the initial value and return to step 3. In the present gradient cycle, $\varepsilon=0.01$ and $|(f(\vec{h}_{k+1})-f(\vec{h}_k))/f(\vec{h}_{k+1})|=0.297 > \varepsilon$. The iteration continues from step 3.

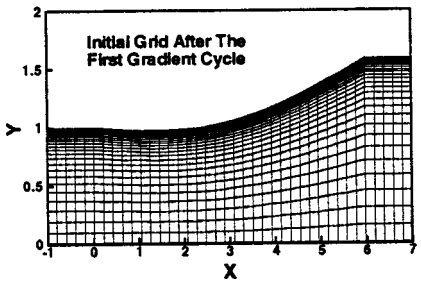

Fig. 15 Initial diffuser shape and grid after the first gradient cycle

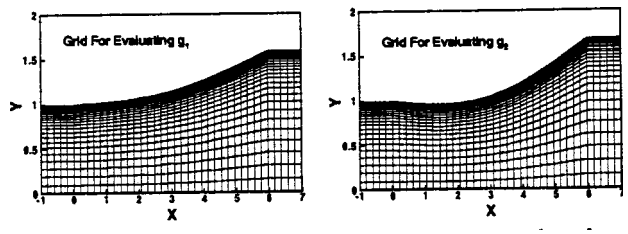

Fig. 16 Diffuser shapes and grids for evaluating gradient vector

References

[1] Japikse, D., and Baines, N. C., 1998, *Diffuser Design Technology*, Concepts ETI, Inc.

[2] Bein, T. W., and Lee, Y. T., 1999, ''Performance Evaluation of an Air-Conditioning Compressor, Part I: Measurement and Design Modeling,'' International J. of Rotating Machinery, **5**, No. 4, pp. 231–240.

[3] Lee, Y. T., and Bein, T. W., 1999, ''Performance Evaluation of an Air-Conditioning Compressor, Part II: Volute Flow Predictions,'' International J. of Rotating Machinery, **5**, No. 4, pp. 241–250.

[4] Baysal, O., and Eleshaky, M. E., 1991, ''Aerodynamic Sensitivity Analysis Methods for the Compressible Euler Equations,'' ASME J. Fluids Eng., **113**, pp. 681–688.

[5] Reuther, J., and Jameson, A., 1995, ''Supersonic Wing and Wing-Body Shape Optimization using an Adjoint Formulation,'' *CFD for Design and Optimization*, ASME FED-Vol. 232, pp. 45–52.

[6] Cabuk, H., and Modi, V., 1992, ''Optimum Plane Diffusers in Laminar Flow,'' J. Fluid Mech., **237**, pp. 373–393.

[7] Zhang, J., Chu, C. K., and Modi, V., 1995, ''Design of Plane Diffusers in Turbulent Flow,'' *Inverse Problems in Engineering*, **2**, Overseas Publishers Association, pp. 85–102.

[8] Panting, J. R., 1998, *Optimizing the Super-turbocharged Aeroengine*, Professional Engineering Publishing Limited, London.

[9] Mrsa, Z., 1998, ''A Turbulent Flow Shape Optimization Method for Nozzle Design,'' Computational Technologies for Fluid/Thermal/Structural/Chemical Systems With Industrial Applications, Vol. II, ASME PVP-Vol. 377-2, pp. 87–92.

[10] Koller, U., Monig, R., Kusters, B., and Schreiber, H., 2000, ''Development of Advanced Compressor Airfoils for Heavy-Duty Gas Turbines, Part I: Design and Optimization,'' ASME J. Turbomach., **122**, pp. 397–405.

[11] Press, W. H., Flammery, B. P., Teukolsky, S. A., and Vetterling, W. T., 1989, *Numerical Recipes, The Art of Scientific Computing*, Cambridge University Press.

[12] Polak, E., 1971, *Computational Methods in Optimization*, Academic Press, New York, Sec. 2.3.

[13] Nelder, J. A., and Mead, R., 1965, ''A Simplex Method for Function Minimization,'' Comput. J. (UK), **7**, pp. 308–313.

[14] Acton, F.S., 1973, *Algorithms for Minimization Without Derivatives*, Prentice-Hall, Englewood Cliffs, NJ, Chap. 7.

[15] Chen, Y. S., 1989, ''Compressible and Incompressible Flow Computations With a Pressure Based Method,'' Paper No. AIAA-89-0286.

Discussion: ''Direct Method for Optimization of a Centrifugal Compressor Vaneless Diffuser'' (Lee, Y.-T., Luo, L., and Bein, T. W., 2001, ASME J. Turbomach., 123, pp. 73–79)

N. A. Cumpsty
Chief Technologist, Rolls-Royce plc, PO Box 31, Derby DE24 8BJ, United Kingdom

I found this an interesting and original paper. Although I do not pretend to understand the details of the optimization procedure, I am interested in the predictions, and one aspect of the results does surprise me. I would have expected the optimum annulus shape to be markedly different depending on whether the optimization was for minimizing loss in stagnation pressure or maximizing rise in static pressure. I am therefore surprised that the shapes of the annulus are so similar in Fig. 7 for the different optimization weightings; it does not seem to make much difference whether the static pressure rise Cp or the total pressure loss w are optimized. Similarly, I am surprised that the values of predicted static pressure rise coefficient Cp and stagnation pressure loss coefficient w are almost equal for different optimizations, though substantially better than for the datum diffuser. What does this tell us about the optimization process and about the flow that is being studied?

One of the least desirable features of the datum diffuser seems

to be the sudden area increase near its exit. Is it possible that the improvement in performance of the optimized diffusers comes primarily from eliminating this feature?

We are told that the compressor volute has very poor performance; in other words the pressure rise in the volute downstream of the diffuser will contribute relatively little to the overall machine efficiency and pressure rise. In that case would it not have been more appropriate for this diffuser to have optimized only on static pressure rise and ignore the loss in the diffuser?

Closure to ''Discussion of 'Direction Method for Optimization of a Centrifugal Compressor Vaneless Diffuser''' (2001, ASME, J. Turbomach., 123, p. 79)

Yu-Tai Lee, Lin Luo, and Thomas W. Bein

The point made by Professor Cumpsty concerning the results related to the variation of the weighting coefficients shown in Fig. 7 is well taken. We found that the figure's legend was misplaced in the pamphlet paper; we have redrawn Fig. 7. If the stagnation pressure is approximated by $p_t = p_s + 1/2\rho u^2$, the objective functions searched by the three sets of weighting coefficients shown in Fig. 7 are

$$f(h) = \min(\Delta p_s + \Delta p_t) = \min(\Delta p_s + \Delta p_s + \Delta(1/2\rho u^2)) = \min(2\Delta p_s + \Delta(1/2\rho u^2))$$

for $\alpha=1$ and $\beta=1$, and

$$f(h) = \min(\Delta p_s + 3\Delta p_t) = \min(\Delta p_s + 3\Delta p_s + 3\Delta(1/2\rho u^2)) = \min(4\Delta p_s + 3\Delta(1/2\rho u^2))$$

for $\alpha=1$ and $\beta=3$, and

$$f(h) = \min(3\Delta p_s + \Delta p_t) = \min(3\Delta p_s + \Delta p_s + \Delta(1/2\rho u^2)) = \min(4\Delta p_s + \Delta(1/2\rho u^2))$$

for $\alpha=3$ and $\beta=1$. The weighting coefficients for the static pressure rise term of the last two calculations ($\alpha=1$, $\beta=3$ and $\alpha=3$, $\beta=1$) are identical, although the coefficients for the dynamic head are 3 versus 1. Similarly the dynamic-head coefficients between $\alpha=1$, $\beta=1$ and $\alpha=3$, $\beta=1$ are identical and the pressure rise coefficients are 2 versus 4. The three cases investigated in Fig. 1 have much less impact from the changes of the weighting coefficients than the limiting case with $\alpha=1$ and $\beta=0$. In addition, for the current diffuser, the gains from C_p and ω are comparable in their magnitudes between the original and the other cases. Therefore, the end configurations are less dependent on the coefficients used and very close to each other.

Certainly the original diffuser outlet shape plays some role in the final result, but it is not the sole contribution. Both Figs. 10 and 12 show that the gain in the loss reduction is mainly from the front section of the diffuser and the gain in the pressure recovery is mainly from the rear half of the diffuser, but not just from the last 5 percent of the diffuser length.

Although the attached volute of the present compressor does not perform well, the gain in pressure recovery from the diffuser shown in Fig. 1 is 35.9 percent between the original and the case with $\alpha=\beta=1$. Similarly, the loss reduction is reduced by 24.3 percent. The resultant shape will be different from the current optimized shape if the coefficients are set as $\alpha=1$ and $\beta=0$. The advantage of selecting $\alpha=1$ and $\beta=0$ is to achieve a higher pressure rise. However, the flow separation shown in Fig. 10 may become pronounced due to lack of control in loss used in the optimization calculation and eventually the stall occurs much earlier than under the original conditions.

